Soft Matter

PAPER

View Article Online
View Journal

Cite this: DOI: 10.1039/c6sm01946c

Shear-driven segregation of dry granular materials with different friction coefficients

Katalin A. Gillemot,* Ellák Somfai and Tamás Börzsönyi

Received 23rd August 2016,
Accepted 22nd November 2016

DOI: 10.1039/c6sm01946c

www.rsc.org/softmatter

We report the first experimental demonstration of bulk segregation in a shear-driven dry granular mixture, where the particles only differ in their surface friction coefficients. We found that the smoother particles tend to sink to the bottom of the shear zone, while rough particles migrate to the top of the sample. This phenomenon is similar to the well known kinetic sieving in particle mixtures with size heterogeneity. In the present case the smooth particles have a higher probability to penetrate into voids created by the shearing than the rough ones. Discrete element simulations were carried out and reproduced the experimentally observed segregation patterns. Moreover, simulations performed in the absence of gravity revealed that rough particles tend to remain in the shear zone, while the smooth particles are being expelled from it. We propose a mechanism in which the smooth particles are driven towards regions of lower shear rate.

1 Introduction

Segregation phenomena in granular materials are very complex, and their prediction is often challenging.[1–3] An efficient mixing or demixing of materials is highly desirable in industry, while in nature, *e.g.* in geological processes, segregation often plays a key role.

Granular mixtures subjected to flow or vibration can segregate due to differences in grain size, density, shape or surface properties. Size[4–15] and density[15–17] segregation are both well known and well investigated; however less attention has been given to further effects like segregation due to differing particle shapes[18–21] or the diversity in the surface friction coefficients of the particles, the case we wish to discuss in the current paper. Furthermore different external conditions (like system geometry, filling rate, particle-wall friction coefficient) or various driving forces (like vibration or shear) may invoke different segregation mechanisms (for example kinetic sieving[6] or convection[7]), and in the real world it is highly likely that a combination of these conditions exists, causing complex spatial patterns that are not easily explained. One example is the sharp transition from the reverse Brazil nut effect to the Brazil nut effect observed in vibrated granular mixtures, assumed to be caused by aging of the particles resulting in a drift in their friction coefficients.[22]

Segregation in surface flows has been observed due to the different angles of repose (internal friction) of the constituents arising from grain shape differences and/or microscopic surface roughness. In an early experiment Zik *et al.* investigated axial segregation (banding) of binary mixtures of sand and glass beads of similar grain size in a rotating tube.[23] They have already concluded that the size difference between the particles itself would not be enough to induce the observed segregation, but their shape and surface roughness also play an essential role. Using the model proposed by Bak *et al.*,[24] Lai *et al.*[25] found that in a rotating drum radial segregation occurs. Similarly, effects of the angle of repose differences (caused by grain shape variations) were investigated theoretically in heap flows by Makse.[18] Using a granular-media lattice gas model Károlyi *et al.* have also detected segregation when filling a silo,[26] with the smooth particles accumulating at the base of the pile. By applying different system geometries in their numerical models both Bantang *et al.*[27] and Farkas *et al.*[28] were able to efficiently separate particles with different angles of repose. Interestingly enough when it finally came to experiments by using quasi-two and -three dimensional rotating tumblers Pohlmann *et al.*[29] have found no trace of radial segregation or banding for bidisperse mixtures of rough and smooth particles. Furthermore, changing the surface roughness of a single intruder particle in a pool of similar particles can change its dynamics.[30,31]

Due to the difficulty of fabricating samples where only the surface roughness of the particles differs while their size, density and shape are kept unchanged, the problem of surface friction-difference induced bulk segregation could be tackled typically mostly in numerical simulations[30–33] or analytically.[34] A vibrating system was investigated by Ciamarra *et al.*[32] using discrete element simulations. In this case the two components segregated in the bulk with the rough particles rising towards the top of the system. In a granular mixture immersed in a

Institute for Solid State Physics and Optics, Wigner Research Center for Physics, Hungarian Academy of Sciences, P.O. Box 49, H-1525 Budapest, Hungary. E-mail: gillemot.katalin@wigner.mta.hu

viscous fluid in a Couette device Plantard *et al.*[33] found that the rough particles accumulate in regions with a higher shear rate. These all highlight the intriguing fact that just as in the case of size segregation, surface roughness driven segregation is a complex and important phenomenon with a strong dependence on the external properties of the system.

In the current paper we focus on the following questions: (1) into which regions do smooth particles migrate in a sheared mixture of dry granular particles, where only the friction coefficients of the particles differ; (2) what happens to the same system in the absence of gravity and (3) what are the mechanisms behind the segregation patterns observed.

2 Methods

The experiments were carried out in a cylindrical split bottom shear cell [shown in Fig. 1(a)] with a radius of $R_{cell} = 52d$, where d is the diameter of the particles. The bottom of the cell consisted of a rotating inner plate with a radius of $R = 41d$ and a static outer ring. The ratio of the filling height H to the radius of the inner plate R was $H/R = 0.48$, resulting in a mostly radial shear gradient in the region indicated by red in Fig. 1(a). The rotation speed was 1.2 rpm resulting in quasistatic shear. The whole bottom area of the cell was roughened in order to minimize crystallization of the grains.

High precision ABS plastic spheres were used with an average diameter of $d = 5.953$ mm and a mass of 0.12 g. We have measured the diameter of 500 beads with a digital caliper (resolution 0.01 mm), and these measurements yielded a polydispersity of 0.6% for the smooth beads. Half of the sample was roughened with an apparatus designed exclusively for this purpose. During the roughening process the beads were gently compressed between two rough surfaces with a nominal roughness of 0.2 mm and the surfaces were moved tangentially with respect to each other. This way the beads were rolling during compression, and depressions were created all over their surface [see Fig. 1(b)] without rubbing any material away, and thus without changing the size or the density of the particles. These roughened particles were then painted by an alcohol based ink; the whole process resulted in an altogether maximum 0.01% gain in particle weight, and 0.05% increase in average diameter (determined again from 500 particles), where the latter was comparable to measurement uncertainty and is much smaller than the measured polydispersity of 0.6%. After roughening the difference between the friction coefficients μ of the two types of particles was determined by measuring their angle of repose α during heap formation. A picture of the heap was recorded after each major avalanching event, and the angle was measured by numerically fitting a line on the middle of the slope of the heap from 1/3rd of its height up to 2/3rd of its height. The averages of the measured angles of repose for the rough and smooth particles are $\bar{\alpha}_R = 23.4^\circ \pm 1.6^\circ$ and $\bar{\alpha}_S = 19.2^\circ \pm 0.9^\circ$ respectively. These correspond to a difference in the friction coefficient $\mu \approx \tan\alpha$ of the two types of grains $\mu_R - \mu_S = 0.433 - 0.348 = 0.085$ [see Fig. 1(e)]. This friction contrast is similar to that obtained by etching glass beads.[35]

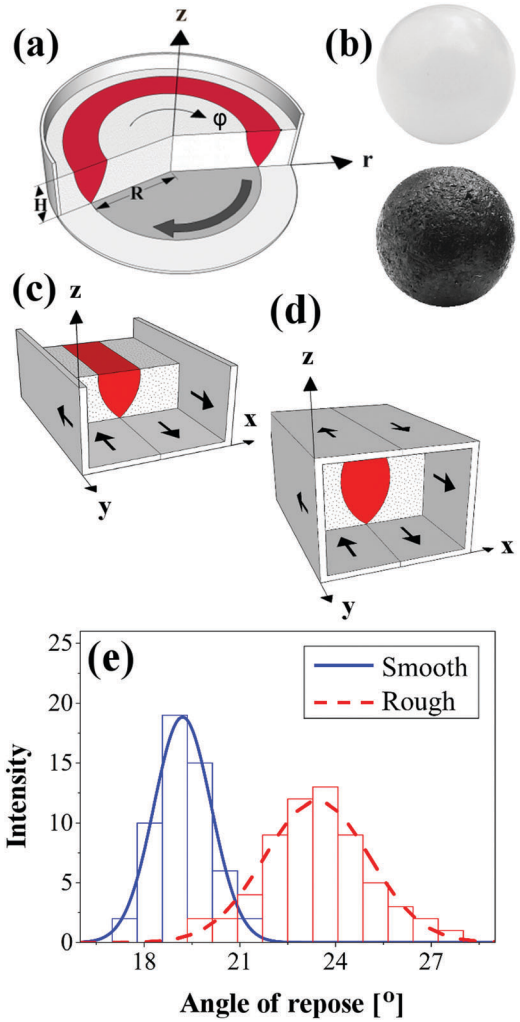

Fig. 1 (a) Schematics of the experimental setup. The shear zone is coloured red. (b) Photograph of a smooth (top, light) and a rough particle (bottom, dark). (c) Schematics of the simulation setup for the gravitational case. (d) Schematics of the simulation setup for the case without gravity. (e) Distributions of the measured angles of repose for the rough and smooth particles, acquired by fitting a Gaussian on the histograms of the measured angle of repose values.

During shearing the surface of the sample was recorded with a Nikon D5100 camera, by taking snapshots at 5 s intervals. After the measurement was stopped the material was excavated layer by layer in order to explore the final segregation pattern inside the sample. This was done by each time removing a sheet of the granular material with a thickness of 20 ± 1 mm and photographing the surface again. The particle removal was done by a specially designed machine with a constant suction power and adjustable height, ensuring that the excavation was controlled. The recorded pictures were then analyzed by counting with a specific detection algorithm the number of the different particles in 2.61 particle wide concentric rings on the given surface.

Altogether two sets of measurements were carried out. (i) First starting with a non-mixed layered configuration, where the smooth particles were layered on top of the rough particles

(labeled "Non-mixed"). For the second measurement the particles were thoroughly mixed beforehand (labeled "Mixed"). We note that in order to minimize the erosion of the surface of the particles the experiments were stopped before the fully segregated steady state was reached. The diameter of 500 rough particles was measured again after the experiments, and a minor (0.12%) decrease of the average diameter was detected.

Extensive numerical calculations were carried out using the discrete element method in order to gain a deeper insight into the dynamics of the system. The simulations were done using the LIGGGHTS package[36] with the contact force based on the Hertz–Mindlin contact model of sliding friction; a detailed description of the particular model can be found in ref. 36. In addition, we also made tests with rolling friction included as well, and have found no significant change in the system behaviour. The particles used had no polydispersity in order to avoid size segregation. The friction coefficients were $\mu_{RS} = 0.5$, $\mu_{RR} = 0.6$, $\mu_{SS} = 0.4$, $\mu_{RW} = 0.55$, and $\mu_{SW} = 0.45$, where the indicies indicate the type of particle pairs: R for rough, S for smooth, and W for wall particles. However we also made tests with both smaller and larger roughness differences resulting in the same segregation pattern, but on different timescales. Two types of simulations were performed: (i) in the presence of gravity a linear split bottom geometry was modeled by two L-shaped walls [see Fig. 1(c)] and a size of $28 \times 13 \times 12$ particle diameters. The top of the box was covered with a frictionless static wall to keep the particles inside, and boundary conditions in the shear direction were periodic. The box was filled to result in a free surface on the top, and during the simulations we found an average volume fraction of $\phi = 0.63$ in the shear zone. (ii) In the absence of gravity we used a double split geometry in order to avoid effects caused by the static wall on the top. Here two U shaped walls formed the two splits at the bottom and top of the cell [see Fig. 1(d)]. The cell size was once again $28 \times 13 \times 12$ particle diameters, and filled to result in an average volume fraction of $\phi = 0.63$. Furthermore we have also tested several cases with ϕ down to 0.54 and up to 0.65 and found the same segregation patterns as described below. In both cases volume control was imposed on the system. The walls were made of slightly overlapping particles glued together, and they were moving with a constant speed, but in opposite directions along the y axis shearing the system. To avoid the effects of the initial transient, a sample of identical particles was sheared at first, and only then the two different friction coefficients were assigned to particles at random to start the real measurements. The simulation parameters were set up so that the inertial number was in the range of $0.0001 < I < 0.003$, corresponding to the quasistatic regime. Any physical quantities were then extracted from the simulations by making an ensemble average over the particles found in $1 \times 1 \times 1$ particle diameter sized bins in the simulation space.

3 Results and discussion

First we present the experimental results obtained in the cylindrical split bottom shear cell. Fig. 2(a) and (d) depict the time evolution of the radial particle distribution on the surface of the sample focusing on the transient region, for both the initially layered Non-mixed and the Mixed cases respectively. Here, the difference between the number fraction of the rough n_R and smooth n_S particles (the number density of one type normalized by the total number density) is averaged along the angular coordinate, *i.e.*

$$\delta n_H(r,t) = \langle (n_R - n_S)|_{z=H} \rangle_\varphi,$$

where r, z and φ are the radial, vertical and angular coordinates, respectively and t is the time. After the initial mixing of the particles we can see a clear accumulation of rough particles on the surface with a nonuniform spatial distribution, with two maxima developing at the two sides of the shear zone. While in the Mixed case the two maxima are clearly distinguishable, in the Non-mixed case the second maximum is only starting to develop. Here we note again that we did not wait until the system reaches the fully developed stationary state, since the process was slow compared to the erosion of the beads. This allowed us to perform these two subsequent experiments with the same sample. On one hand erosion of the grains leads to decreasing optical contrast between the two types of grains due to the smudging of the paint, and thus identifying smooth and rough particles becomes increasingly difficult. On the other hand erosion also leads to slow degradation of the friction contrast between the grains.

In Fig. 2(b) and (e) the full time dependence of δn_H is shown, averaged over different concentric rings on the surface. The black curve (labeled "r1") corresponds to the innermost circle (see top of Fig. 2(c) and (f)), while the green curve (labeled "r5") to the outermost ring, and the rest of the curves cover up the shear zone itself. While the particle distribution of the innermost circle changes only slightly during the experiments, the outermost ring starts to accumulate rough particles after a certain time. This asymmetry and the fact that the inner side of the shear zone (red curve, labeled "r2") accumulates the most rough particles is probably associated with the circular nature of the cell. One more thing to note is that the ring covering the middle of the shear zone (blue curve, labeled "r3") is the first to start to fill up with rough particles, but starts mixing again before an equilibrium state is reached, a phenomenon probably associated with the secondary flow in the system discussed later. As mentioned earlier there is clear accumulation of rough particles with two maxima on the top of the sample for the Mixed case (see Fig. 2(e), red and yellow curves, labeled "r2" and "r4" respectively). In the Non-mixed case – due to the termination of the experiments before the equilibrium state is reached – this second maximum has not yet developed. However from the increase of the yellow curve (labeled "r4", corresponding to the outer side of the zone) and the decrease of the blue curve (labeled "r3", corresponding to the center of the zone) in Fig. 2(b) it is expected that this second maximum would be built later, just as it happened in the Mixed case.

Fig. 2(c) and (f) show the averaged vertical cross section of the sample at the end of the experiments, once the shearing was stopped. The difference in particle numbers is now:

$$\delta n_T(r,z) = \langle (n_R - n_S)|_{t=T} \rangle_\varphi,$$

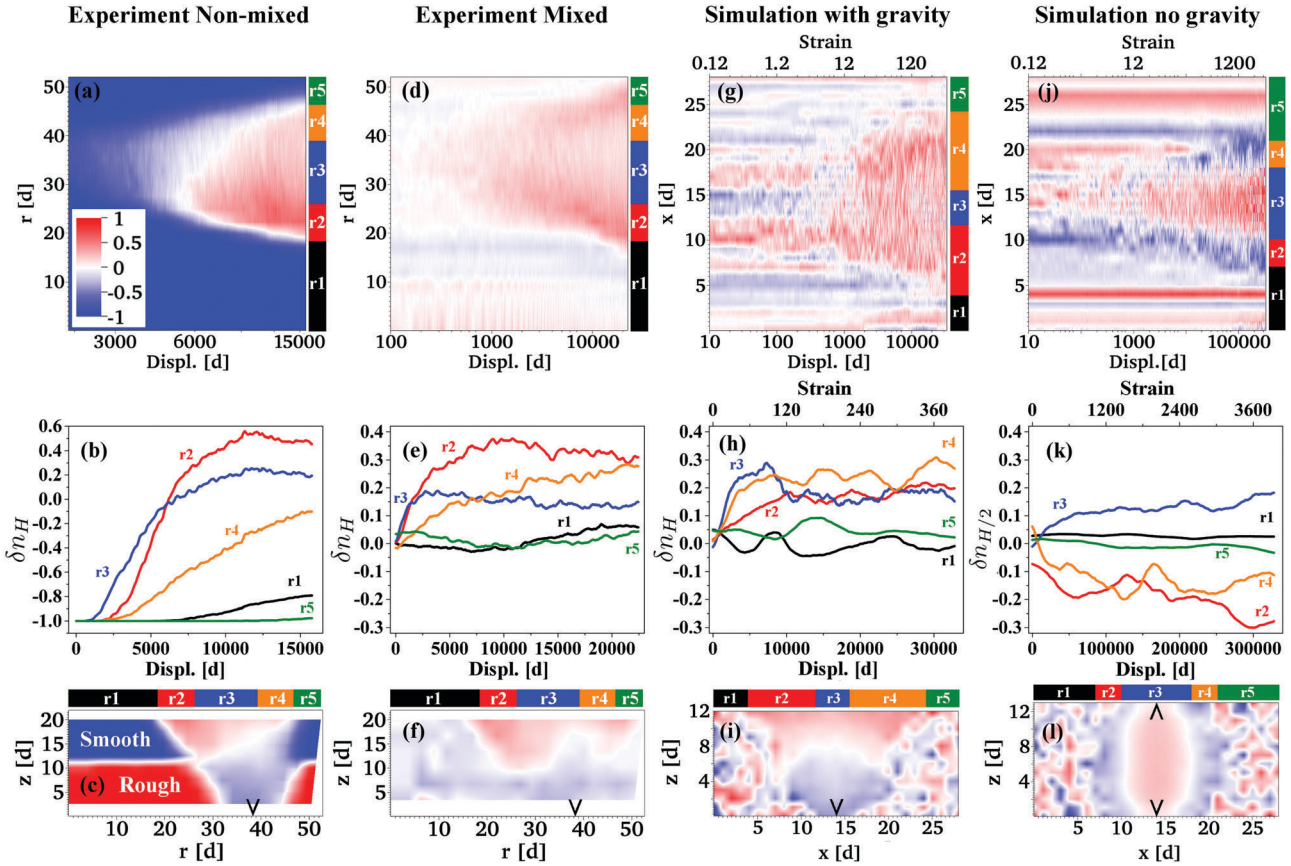

Fig. 2 (a, d, g, j) Particle distribution as a function of displacement between the two sides of the shearzone (in particle diameter units) on the surface of the sample ($z = H$) for (a), (d) and (g), and at the middle of the sample ($z = H/2$) for (j), pictured on a log scale, thus showing mostly the transient region. The red colour on the graphs shows that $\delta n > 0$, meaning that there are more rough particles in that particular area, while blue is $\delta n < 0$ meaning an accumulation of smooth particles. The colour scale is only shown in (a), but corresponds to all pictures. (b, e, h, k) Particle distribution as a function of the displacement of the two sides of the shearzone summed up for different concentric rings on the surface of the sample ($z = H$) for (b), (e) and (h), and at the middle of the sample ($z = H/2$) for (k). The black curve (labeled "r1") corresponds to the innermost circle, while the green curve (labeled "r5") to the outermost ring. The colour-legend for the curves, showing their exact spatial extent can be found next to the top row plots and also above the bottom row of plots. As a reference the cumulative strain is shown on the top axis of the simulation plots: measured at the middle of the top lid for (g), (h) and in the middle of the simulation box for (j), (k). (c, f, i, l) Spatial distribution of the particles in the cross section of the cell, the colour scale is the same as in (a). The black triangles show the exact location of the split. (a–c) Experiment started from the Non-mixed initial condition. (d–f) Experiment started from the Mixed initial condition. (g–i) Numerical simulation with gravity. (j–l) Numerical simulation without gravity. We note here that in order to better visualize the discrete results from counting the particles a set of further datapoints were linearly interpolated onto the graphs in spatial directions.

where T is the time when the rotation was stopped. Once again we can see in both the Non-mixed and Mixed cases the clear accumulation of the rough particles on the surface, but now we can also note that the two density maxima of rough particles observed at the surface corresponds to deeper regions at those radii. The smooth particles on the other hand concentrate at the bottom of the shear zone, near the split (indicated with a wedge). This effect is less dominant in the Mixed case most probably due to the particles losing their difference in surface friction coefficients during the experiments. The material exchange takes place solely in the shear zone, while outside the zone the initial configuration is mostly preserved.

Numerical simulations provide further insight, as monitoring the evolution inside the sample as well as turning gravity on/off is easily feasible. In order to directly compare the simulation results to the experiments we have plotted the same quantities in Fig. 2(g)–(i) as in Fig. 2(d)–(f). Both the time evolution at the surface and the resulting spatial patterns are very similar to the experimental observations. The rough particles accumulate at the top of the shear zone while the smooth particles sink to the bottom. Once again the upper central region of the shear zone accumulates rough particles the fastest (blue curve, labeled "r3"), but after the initial increase the curve slightly decreases as also seen in the experiments. Furthermore we can see the two regions at the two sides of the shear zone with a higher number of rough particles just as in the experimental cell. For simplicity in the simulations we have used a straight shear cell (instead of the cylindrical geometry), such that the resulting pattern (x–z plane) is symmetric [Fig. 2(i)].

To test the effect of gravity a further set of simulations has been performed in the absence of a gravitational force. In this case the setup was slightly modified as two splits were included on the opposite sides of the system. This resulted in a simpler, more symmetric shear zone, making the interpretation of the result

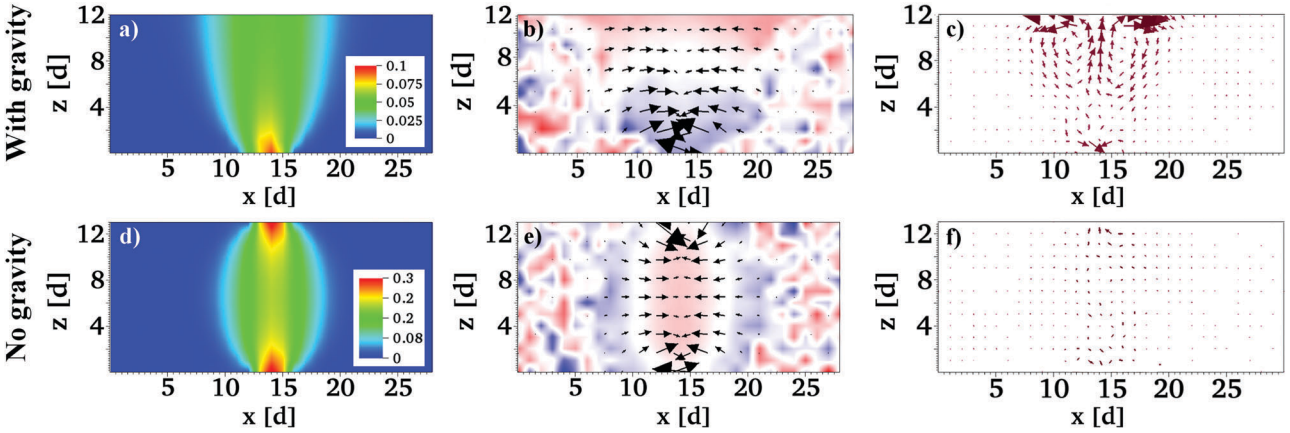

Fig. 3 Numerical results. (a–c) Gravitational case. (a) Shear rate. (b) Gradient of the shear rate (black vectors) plotted over the averaged particle distribution. (c) Secondary flow observed when gravity is on. (d–f) Gravity is turned off. (d) Shear gradient. (e) Gradient of the shear rate (black vectors) plotted over the averaged particle distribution. (f) No secondary flow observed, when gravity is off.

more obvious. Now the rough particles accumulate inside the full shear zone, with the smooth particles being expelled from it, resulting in a thin layer of smooth grains around the zone [see Fig. 2(j)–(l)].

Our goal now is to understand the physical origin of the segregation patterns discussed above. In a shear driven, disordered environment the smooth particles have higher mobility, because when experiencing the same force as the rough particles, they have a higher probability of both loosing contact with the particles they were in contact with, as well as penetrating into any void nearby. In the gravitational case the dynamics is dominated by the gravitational force, causing the more mobile smooth particles to percolate downwards inside the zone, resulting in the rough particles being lifted upwards. This is similar to the well known kinetic sieving effect in systems with size heterogenity. In Fig. 3 we plot the averaged vertical x–z cross sections of the simulations. The colours in Fig. 3(a) denote the shear rate, so the shear zone can be identified, whereas the background colours in (b) show the particle distribution δn averaged over time for large times [for the moment ignore the black arrows in (b)]. One can see that inside the shear zone the smooth particles migrated to the bottom, and the rough ones to the top; outside the zone the initial random distribution persisted.

The location of the smooth and rough particles is slightly distorted from a simple layered structure, which we argue is a consequence of a secondary flow. Fig. 3(c) shows the average velocity of the particles within the x–z plane, perpendicular to the primary streamlines. One can identify a vortex pair in the shear zone, driving particles upwards in the middle, and downwards near the edge of the shear zone. The velocities involved are rather small, *e.g.* the upward stream in the middle is about three orders of magnitude smaller than the typical perpendicular shear velocities.† As a consequence, the layer of rough particles on the top is thinner in the middle, and thicker at the sides of the shear zone [Fig. 3(b)]. The effect of this secondary flow is visible in the experiments as well, in the splitting of the rough (red) layer in Fig. 2(f); here we mention again that the asymmetry is due to the curved primary streamlines.

In the absence of gravity neither of the above two mechanisms are operational: there is no body force which would drive the more mobile smooth particles in one direction, and the secondary convection is absent as well [Fig. 3(f)]. Still, we observe that the rough particles end up at a higher concentration in the middle of the shear zone, and the smooth ones form a layer near the edge of the zone. We propose a third mechanism, which is responsible for this pattern in the absence of gravity. In an environment of inhomogenous shear rate, a given particle receives collisions from all directions, but the number of collisions and the amount of fluctuating sideways force are larger from the direction where the shear rate (velocity difference) is larger. Therefore the fluctuating forces push the particles towards regions of smaller shear rates, and the more mobile smooth particles are more susceptible to convert it to displacement. Effectively this is a force pushing smooth particles opposite to the direction of the shear rate gradient. Fig. 3(e) shows the shear rate gradient as arrows; these arrows have the largest magnitude near the borderline separating smooth-rich and rough-rich regions, and their direction is perpendicular to this borderline.

Of the three mechanisms in typical situations the kinetic sieving-based migration of the smooth particles is the strongest, followed by the secondary flow; but these two only operate in the presence of gravity. The third mechanism, based on the anisotropy of fluctuating forces, is present regardless of gravity [see arrows in Fig. 3(b)], but in the presence of gravity it is much weaker and therefore is completely dominated by the other two. In the simulations the segregation pattern in the no-gravity case appears at much later times (much larger deformation) than in the gravitational case.

4 Conclusions

Our experimental and numerical investigations reveal that dry granular particles with different friction coefficients driven by shear segregate inside the shear zone, with the less mobile

† The large arrows at the top of the figure are liable to noise, some of the bins near the surface contained too few particles.

rough particles accumulating on the top of the sample – interestingly in two spatial domains, as a result of a secondary flow – while the more mobile smooth particles sink to the bottom. When switching off gravity in the simulation we found a new and interesting segregation pattern, with the smooth particles being expelled from the shear zone, while the rough ones are being stuck inside. This phenomenon is driven by the asymmetry of fluctuating forces due to the gradient of the shear rate. These results – while highlighting interesting new segregation mechanisms – stress the fact that in order to fully understand complex segregation patterns friction induced segregation may need to be taken into account. As a future step it would be highly intriguing to systematically investigate the segregation patterns found in mixtures of particles with slight shape differences, bridging the gap between roughness and shape driven segregation.

Acknowledgements

The authors would like to thank Balázs Szabó and Dávid Visontai for the numerous discussions, Viktor Kenderesi for technical assistance, and the National Information Infrastructure Development Institute for awarding us access to resources based in Hungary at Budapest, Debrecen, Szeged and Miskolc. Financial support from the Hungarian Scientific Research Fund (Grant No. OTKA NN 107737) and the János Bolyai Research Scholarship and the Postdoctoral Scholarship of the Hungarian Academy of Sciences is also acknowledged.

References

1 I. S. Aranson and L. S. Tsimring, *Rev. Mod. Phys.*, 2006, **78**, 641–692.
2 P. Richard and N. Taberlet, *Soft Matter*, 2008, **4**, 1345–1348.
3 C. R. K. Windows-Yule, B. J. Scheper, A. J. van der Horn, N. Hainsworth, J. Saunders, D. J. Parker and A. R. Thornton, *New J. Phys.*, 2016, **18**, 023013.
4 J. Williams and G. Shields, *Powder Technol.*, 1967, **1**, 134–142.
5 A. Rosato, K. J. Strandburg, F. Prinz and R. H. Swendsen, *Phys. Rev. Lett.*, 1987, **58**, 1038–1040.
6 S. B. Savage and C. K. K. Lun, *J. Fluid Mech.*, 1988, **189**, 311–335.
7 J. B. Knight, H. M. Jaeger and S. R. Nagel, *Phys. Rev. Lett.*, 1993, **70**, 3728–3731.
8 E. Clément, J. Rajchenbach and J. Duran, *Europhys. Lett.*, 1995, **30**, 7–12.
9 F. Cantelaube and D. Bideau, *Europhys. Lett.*, 1995, **30**, 133–138.
10 H. A. Makse, S. Havlin, P. R. King and H. E. Stanley, *Nature*, 1997, **386**, 379–382.
11 L. Naji and R. Stannarius, *Phys. Rev. E: Stat., Nonlinear, Soft Matter Phys.*, 2009, **79**, 1–8.
12 K. Hu, Z.-A. Xie, P. Wu, J. Sun, L. Li, C. Jia, S. Zhang, C. Liu and L. Wang, *Soft Matter*, 2014, **10**, 4348–4359.
13 C. P. Schlick, Y. Fan, P. B. Umbanhowar, J. M. Ottino and R. M. Lueptow, *J. Fluid Mech.*, 2015, **765**, 632–652.
14 P. Gajjar, K. van der Vaart, A. R. Thornton, C. G. Johnson, C. Ancey and J. M. N. T. Gray, *J. Fluid Mech.*, 2016, **794**, 460–505.
15 Y. Fan and K. M. Hill, *Phys. Rev. E: Stat., Nonlinear, Soft Matter Phys.*, 2010, **81**, 041303.
16 T. Shinbrot and F. J. Muzzio, *Phys. Rev. Lett.*, 1998, **81**, 4365–4368.
17 N. Thomas, *Phys. Rev. E: Stat. Phys., Plasmas, Fluids, Relat. Interdiscip. Top.*, 2000, **62**, 961–974.
18 H. A. Makse, *Phys. Rev. E: Stat. Phys., Plasmas, Fluids, Relat. Interdiscip. Top.*, 1997, **56**, 7008–7016.
19 C. R. Abreu, F. W. Tavares and M. Castier, *Powder Technol.*, 2003, **134**, 167–180.
20 A. V. Kyrylyuk, M. A. van de Haar, L. Rossi, A. Wouterse and A. P. Philipse, *Soft Matter*, 2011, **7**, 1671.
21 A. Shimoska, I. Nousou, Y. Shirakawa and J. Hidaka, *Chem. Eng. Trans.*, 2013, **32**, 2143–2148.
22 S. Ulrich, M. Schröter and H. L. Swinney, *Phys. Rev. E: Stat., Nonlinear, Soft Matter Phys.*, 2007, **76**, 042301.
23 O. Zik, D. Levine, S. G. Lipson, S. Shtrikman and J. Stavans, *Phys. Rev. Lett.*, 1994, **73**, 644–647.
24 P. Bak, C. Tang and K. Wiesenfeld, *Phys. Rev. Lett.*, 1987, **59**, 381–384.
25 P. Y. Lai, L.-C. Jia and C. K. Chan, *Phys. Rev. Lett.*, 1997, **79**, 4994.
26 A. Károlyi, J. Kertész, S. Havlin, H. A. Makse and H. E. Stanley, *Europhys. Lett.*, 1998, **44**, 386–392.
27 J. Bantang, M. Lim, C. Monterola and C. Saloma, *Phys. Rev. E: Stat., Nonlinear, Soft Matter Phys.*, 2002, **66**, 041306.
28 Z. Farkas, F. Szalai, D. E. Wolf and T. Vicsek, *Phys. Rev. E: Stat., Nonlinear, Soft Matter Phys.*, 2002, **65**, 022301.
29 N. A. Pohlman, B. L. Severson, J. M. Ottino and R. M. Lueptow, *Phys. Rev. E: Stat., Nonlinear, Soft Matter Phys.*, 2006, **73**, 031304.
30 C. C. Liao, S. S. Hsiau and C. S. Wu, *Phys. Rev. E: Stat., Nonlinear, Soft Matter Phys.*, 2012, **86**, 061316.
31 C.-C. Liao, S.-S. Hsiau and C.-S. Wu, *Powder Technol.*, 2014, **253**, 561–567.
32 M. P. Ciamarra, M. D. De Vizia, A. Fierro, M. Tarzia, A. Coniglio and M. Nicodemi, *Phys. Rev. Lett.*, 2006, **96**, 058001.
33 G. Plantard, H. Saadaoui, P. Snabre and B. Pouligny, *Europhys. Lett.*, 2006, **75**, 335–341.
34 Y. Srebro and D. Levine, *Phys. Rev. E: Stat., Nonlinear, Soft Matter Phys.*, 2003, **68**, 061301.
35 S. Utermann, P. Aurin, M. Benderoth, C. Fischer and M. Schröter, *Phys. Rev. E: Stat., Nonlinear, Soft Matter Phys.*, 2011, **84**, 1–9.
36 C. Kloss, C. Goniva, A. Hager, S. Amberger and S. Pirker, *Prog. Comput. Fluid Dyn.*, 2012, **12**, 140–152.

